A FAST METHOD FOR GENERATING HIGH-RESOLUTION SINGLE-FREQUENCY SEISMIC ATTRIBUTES

MOHAMMAD RADAD, ALI GHOLAMI and HAMID REZA SIAHKOOHI

Institute of Geophysics, University of Tehran, Iran.
mradad@ut.ac.ir; agholami@ut.ac.ir; hamid@ut.ac.ir

(Received April 23, 2015; revised version accepted October 22, 2015)

ABSTRACT

Radad, M., Gholami, A. and Siahkoohi, H.R., 2016. A fast method for generating high-resolution single-frequency seismic attributes. *Journal of Seismic Exploration*, 25: 11-25.

Single-frequency seismic attributes play an important role in seismic data interpretation. The resolution of single-frequency seismic sections and the run time for generating them are two main factors which need significant attention when dealing with large seismic data sets. In this paper, using the Fourier domain formulation of time-frequency analysis, we formulate the problem of extracting a single-frequency section from time-frequency representation of the data, without requiring the analysis of all frequencies. Furthermore, using an optimization algorithm based on maximum energy concentration, a method is proposed for automatic adjustment of the width of window required for extracting local information around the desired frequency. Application on 2D and 3D seismic data sets for detecting low-frequency shadow of gas-bearing zones and channel detection confirmed the high performance of the proposed method and its efficiency compared to conventional time-frequency based techniques like standard S-transform.

KEY WORDS: single-frequency, energy concentration, seismic attribute, gas and channel detection.

INTRODUCTION

Spectral variation in seismic data can be due to geological events such as probable changes in stratigraphic conditions like channels or hydrocarbon accumulation. For studying these cases, single-frequency seismic attribute, as an interpretation tool, has been utilized in many researches for several years (e.g., Herrera et al., 2014; Xue et al., 2013; Liu et al., 2011; Wu and Liu, 2009; Liu, 2006; Castagna et al., 2003). To extract a single-frequency data set from a seismic data set, the time-frequency (TF) analysis of the data is needed.

0963-0651/16/$5.00

For this aim, several TF representation (TFR) methods have been employed such as short-time Fourier transform (STFT) (Gholami, 2013), Wigner-type energy distribution (Wu and Liu, 2009), wavelets (Sinha et al., 2005), S-transform (Zhang, 2011) matching pursuit decomposition (Wang, 2010; Wang 2007) and Hilbert-Haung transform (Herrera et al., 2014; Xue et al., 2013). Obviously, a high-resolution TFR method will yield more accurate results. One of the efficient techniques to improve the resolution of TFR methods is using the energy concentration concept (Gholami, 2013; Djurovic et al., 2008, Stankovic, 2001; Jones and Parks, 1990). The remedy is to determine window width for a Fourier-based TFR method using an optimization algorithm to maximize the energy concentration of the TF plane. Based on this approach, Gholami (2013) found an optimum window width employed for the entire TF plane. Later on Sattari et al. (2013) used an instantaneous optimization algorithm to find an optimum window width for each time sample of the signal, individually. In this paper, following Gholami (2013) and Sattari et al. (2013), we present an algorithm to find an optimum window width, individually, for each frequency component, instead of each time sample proposed by Sattari et al. (2013). For this purpose, at first, it needs to window the Fourier transform (FT) of signal around each frequency component. Then inverse FT of each segment yields time distribution assigned to the considered frequency. For each frequency sample an optimum window width can be found by using an optimization algorithm and an energy concentration measure. Finally, a high-resolution TF map can be obtained by employing the optimum windows. The remarkable advantage of our method is its efficiency in providing high-resolution single-frequency data set in a fast process. To have a high-resolution single-frequency data set by the TFR method proposed by Sattari et al. (2013), it is needed to transform the whole seismic data to TF domain by analyzing the entire seismic trace. Then it would be possible to produce a single-frequency data set by slicing at a special frequency component. However, since seismic data are usually large-scale, this technique needs great computational costs. However, by our method, for generating a single-frequency data set, there is no necessity to perform a complete TF analysis of each trace. It means that it is not necessary to transform the whole FT of the trace to the TF domain. It is sufficient to perform the optimization process just for the interested frequency component to find the optimum window width. Therefore, besides generating a high-resolution single-frequency seismic attribute, the computational costs will be reduced, significantly.

After presenting a theoretical background in the next section, we evaluate the performance of the proposed TFR method on a synthetic non-stationary signal for making a high resolution TF map. Then the proposed method is employed on two seismic data sets to detect gas bearing zones, low-frequency shadows and channels using single-frequency attributes. Besides, a complete discussion about computational costs is presented.

THEORETICAL BACKGROUND

High resolution TFR

A Fourier-based TFR of a discrete signal $\mathbf{y}[n] = y(nT)$ with time sampling interval T, can be defined in the matrix form as:

$$\mathbf{TFR} = \mathbf{F}[\mathbf{Y} \odot \mathbf{W}_\sigma] \quad , \tag{1}$$

where $\mathbf{Y}[n,m] = \mathbf{y}[n]$; $\mathbf{W}_\sigma[n,m] = \mathbf{w}_\sigma[n + m - 1]$, for $n,m = 1,\ldots,N$, is a matrix constructed by the shifted versions of a window function $\mathbf{w}_\sigma[n] = w_\sigma(nT)$ and σ is a parameter controlling the window width; $\mathbf{F}$ is the discrete FT (DFT) matrix. The m-th column of TFR is the frequency spectrum of the signal around the m-th time sample. The meaning of $\odot$ is sample by sample multiplication of two matrices.

Eq. (1) in the Fourier domain can be rewritten as:

$$\mathbf{TFR} = \mathbf{F}^{-1}[\hat{\mathbf{Y}} \odot \hat{\mathbf{W}}_\sigma] \quad , \tag{2}$$

where $\hat{\mathbf{Y}}[k,l] = \hat{\mathbf{y}}[k]$, as $\hat{\mathbf{y}}[k]$ is FT of the signal, and $\hat{\mathbf{W}}_\sigma[k,l] = \hat{\mathbf{w}}_\sigma[k+l-1]$ for $k,l = 1,\ldots,N$ is a matrix constructed by the shifted versions of a window function $\hat{\mathbf{w}}_\sigma[k]$. If the partition of unity criteria, $\Sigma_{n=1}^{N}\mathbf{w}_\sigma[n] = 1$, $\forall\sigma$, and $\Sigma_{k=1}^{N}\hat{\mathbf{w}}_\sigma[k] = 1$, $\forall\sigma$ would be satisfied by $\mathbf{w}_\sigma[n]$ and $\hat{\mathbf{w}}_\sigma[k]$, respectively, it can be simply proven that the transforms (1) and (2) will be invertible.

The main factor affecting the TF resolution of Fourier-based TFR methods (1) and (2) is the utilized window. The window shape and width are parameters which control the TF resolution (Pinnegar and Mansinha, 2003). To reach a high resolution TF map based on energy concentration concept, an optimization problem can be defined to find the optimum window parameters as:

$$\underset{\text{window parameters}}{\arg\max \text{ or } \arg\min} \ \mathrm{ECM}(\mathbf{TFR}) \quad , \tag{3}$$

where ECM is a function which measures energy concentration of the TF map. arg max and arg min are optimizers which are chosen based on the type of employed ECM. According to (3), Gholami (2013), found an optimum window width for the entire **TFR**, by measuring energy concentration of the entire TF map. Sattari et al. (2013) employed (3) in an instantaneous scheme to find the optimum window widths for each time sample, individually. In this approach ECM measures energy concentration of frequency spectrum around each time sample. In this paper, the approach considered by Sattari et al. (2013) is called time-domain optimized TFR method which they reach TFR through (1). We solve (3) based on the formulation of (2) where the optimum window parameters

will be found for each frequency component, individually. In this case ECM measures the energy concentration of the time distribution of each frequency component. Here we consider a Gaussian as the window function whose standard deviation represents the window width.

There are several ECMs; Gholami (2013) and Sattari et al. (2013) utilized Log function. Here, we employ the Modified Shannon Entropy to measure the energy concentration of a given distribution $\mathbf{X}$ as (Hurley and Rickard, 2009):

$$\mathrm{ECM}(\mathbf{X}) = -\sum_{\xi} \mathbf{X}_{\xi} \log(\mathbf{X}_{\xi} + \varepsilon)^2 \quad , \tag{4}$$

where ε is a small positive value to prevent the argument of logarithm function from being zero. In the context of this paper, $\mathbf{X}$ is a single-frequency map of a given signal and ξ is the sample index of $\mathbf{X}$. The less value of ECM represents the more energy concentration of the distribution (Hurley and Rickard, 2009). Therefore, in this case, the optimizer in (3) is arg min.

A fast technique to construct a single-frequency seismic data set

If we want to reach a single-frequency seismic data set by the TFR method through (1), at first, it is needed to transform the whole seismic data to a TF domain by analyzing the entire seismic trace. Then making a slice at the intended frequency component generates the single-frequency data set. This procedure is time-consuming, specially when we deal with a large seismic data cube. The run time problem will be even more sever if the aim is to obtain a high resolution single-frequency cube, due to optimization process. Here, we propose a method to reduce the run time, significantly. It is sufficient to perform the optimization process of finding the optimum window width just for the intended frequency component of the data without dealing with other frequencies. Algorithm 1 presents a procedure to obtain a fast high resolution single-frequency data set. In the algorithm, $\hat{\mathbf{W}}^{(k_0)}$ is the window matrix built by using a Gaussian window shifted by frequency sample k_0 and with standard deviation of σ as:

$$\hat{\mathbf{w}}_{\sigma}^{(k_0)}[k] = e^{-(k-k_0)^2/2\sigma^2} \quad . \tag{5}$$

It is worth mentioning that a similar algorithm can be also defined for obtaining single-frequency data set by the standard S-transform (SST) proposed by Stockwell et al. (1996) where the standard deviation of the gaussian window is inversely proportional to frequency. As an example, Fig. 1 shows an illustrative presentation of the fast procedure of generating a single-frequency seismic data set for 40 Hz frequency. As seen in the figure, at first, the seismic data set (a) is Fourier transformed along time axis to attain (b). Then the

windows array (c) with the same size of (a) is constructed by replicating a shifted Gaussian window in the columns. The used gaussian window is shown on (c) in black. A sample by sample multiplication of (b) and (c) yields the local spectra (d) and, finally, (e) as the single-frequency section is obtained by performing the inverse FT on (d) along the frequency axis. To adjust the window width for generating a high resolution single-frequency section it is needed to perform stages (c) to (e) for a set of standard deviations $\sigma_1 < \sigma_2 < \ldots < \sigma_{N_\Pi}$ in order to find the optimum window. The procedure is summarized in Algorithm 1. The standard deviation set is defined such that σ_1 leads to a very narrow (nearly spike) window and σ_{N_Π} leads to a wide window (covering the spectral band of the signal). It is worth mentioning that in Algorithm 1, the optimization stage can be performed by a line search method to reduce run time further. By this approach it will not be necessary to check all the values of $\sigma_i, i=1,\ldots,N_\Pi$ to find the optimum window width.

Algorithm 1: Algorithm of obtaining a fast high resolution single-frequency seismic data set $\mathbf{G}$ at frequency sample k_0. vec reshapes a matrix to a vector.

Initialize:

get a seismic data set $\mathbf{S}$;

choose a set of N_Π possible standard deviations $\sigma_i \in [\sigma_1,\ldots,\sigma_{N_\Pi}]$;

construct $\hat{\mathbf{S}}$ by Fourier transforming $\mathbf{S}$ along the time axis;

For $i = 1 : N_\Pi$

construct $\hat{\mathbf{W}}_{\sigma_i}^{(k_0)}$ as defined in (5);

construct $\mathbf{G}^{(k_0)}$ by inverse Fourier transforming $[\hat{\mathbf{S}} \odot \hat{\mathbf{W}}^{(k_0)}]$;

set: $q(i) = \mathrm{ECM}[\mathrm{vec}(\mathbf{G}^{(k_0)})]$;

End

find the index p minimizing q;

$\hat{\mathbf{W}}_{opt}^{(k_0)} = \hat{\mathbf{W}}_{\sigma_p}^{(k_0)}$;

obtain $\mathbf{G}_{opt}^{(k_0)}$ by inverse Fourier transforming $[\hat{\mathbf{S}} \odot \hat{\mathbf{W}}_{opt}^{(k_0)}]$.

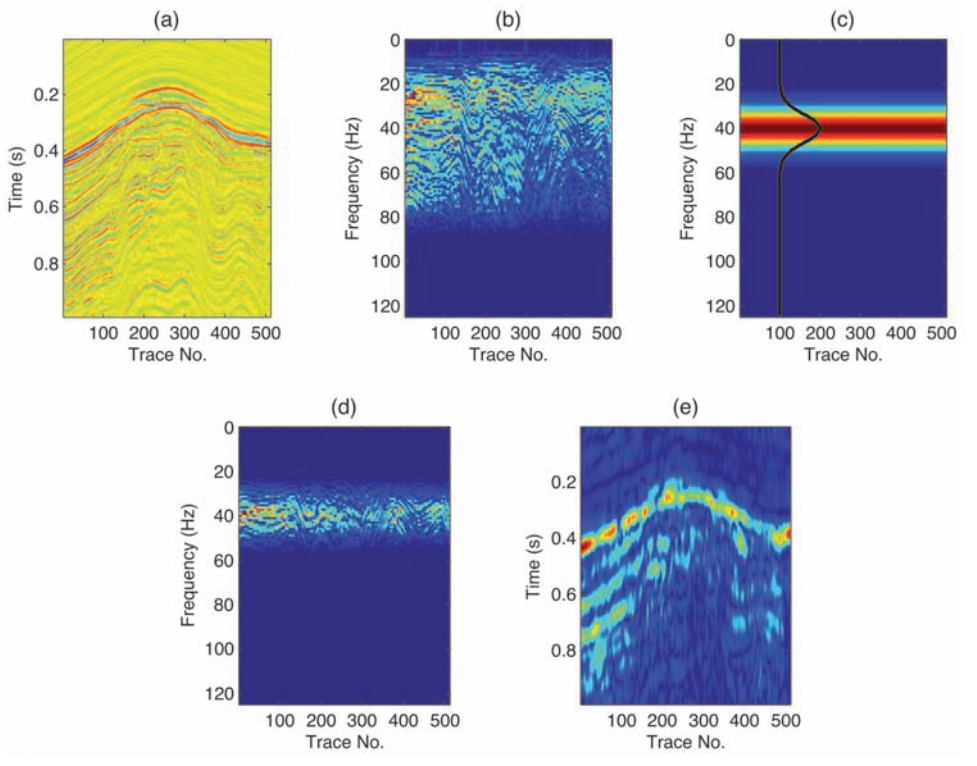

Fig. 1. An illustrative representation of the procedure of generating a single-frequency section. (a) a real seismic data; (b) the FT of (a) along time axis; (c) the windows matrix in FT domain for filtering around frequency 40 Hz. The black curve shows a sample column of the window matrix; (d) local spectra obtained via sample by sample multiplication of (b) and (c); (e) the single-frequency section obtained by inverse FT of (d). Note that, (b), (c), and (d) show the magnitude of the complex coefficients.

IMPLEMENTATION

TFR of synthetic signal

Figs. 2(a) and 2(b) show a synthetic signal and its amplitude spectrum. The TFRs of the signal determined by SST and the proposed method are shown in Figs. 2(c) and (d), respectively. The proposed method is performed for all frequency samples. As seen in the figure, the proposed method [Fig. 2(d)] provided a high resolution TF map with more energy concentration than SST [Fig. 2(c)].

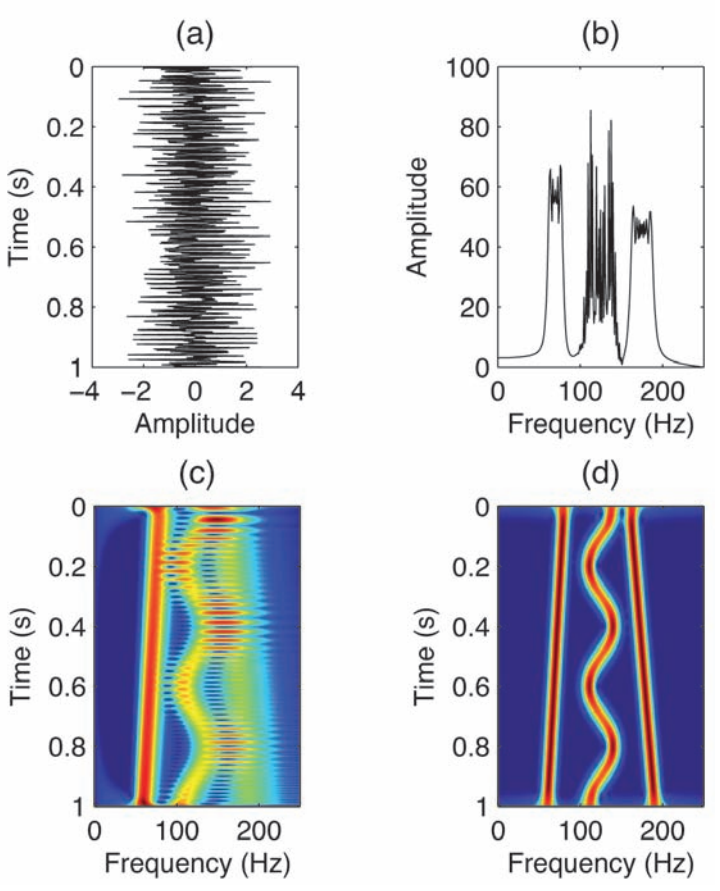

Fig. 2. A non-stationary signal (a) and its amplitude spectrum (b). TFRs of the signal determined by SST and the proposed method are shown in (c) and (d), respectively.

Gas and low-frequency shadow detection

The frequency anomaly in seismic data owing to the subsurface condition is caused by attenuation, absorption, overpressure, tuning and fractures (Taner et al., 1979; Taner and Sheriff, 1977; Sinha et al., 2005). Afterwards, some of the geophysical reasons such as normal moveout stretch, deconvolution and incorrect velocity problems can cause frequency anomalies (Barnes, 1992; Yilmaz, 2001). Ebrom (2004) presents several possible mechanisms for low-frequency shadows. The existence of hydrocarbon will also cause attenuation of high-frequency energy in the reservoir, such that the local dominant frequency moves toward the low-frequency range (Dilay and Eastwood, 1995). Taner et al. (1979) noted that the low-frequency zones are associated to gas reservoirs due to anomalous attenuation. Thus, anomalous low-frequency energy is concentrated at or beneath the reservoir level. For

several years, TF analysis of seismic data has been the subject of the numerous researches to detect gas bearing zones and associated low-frequency shadows (e.g., Liu et al., 2011; Deng et al., 2007; Liu et al., 2006; Liu, 2006; Odebeatu, 2006; Sinha et al., 2005). One of the most common techniques in this field of study is using single-frequency attributes to track the spectral variations in different frequencies (e.g., Liu et al. 2011; Liu, 2006; Castagna et al., 2003). In this section, the fast high resolution method presented in Algorithm 1 is applied to a 2D seismic data set to build single-frequency sections for detecting gas bearing zones and low frequency shadows. Also some results are provided by SST and the time-domain optimized TFR methods.

Fig. 3 shows a seismic section from a gas reservoir of Iran. The reservoir level is remarked with white rectangle. The data includes 512 seismic traces with 246 time samples and 4 milliseconds temporal sampling interval. The single-frequency sections for frequencies 15 Hz and 40 Hz determined by SST, the time-domain optimized TFR and the proposed TFR methods are presented in Fig. 4. As seen in the figure, the single-frequency sections obtained by the proposed method [Figs. 4(e) and 4(f)] have higher temporal and spatial resolution and show more details than SST results. The more energy concentration at the reservoir level and also more resolved reflection events in

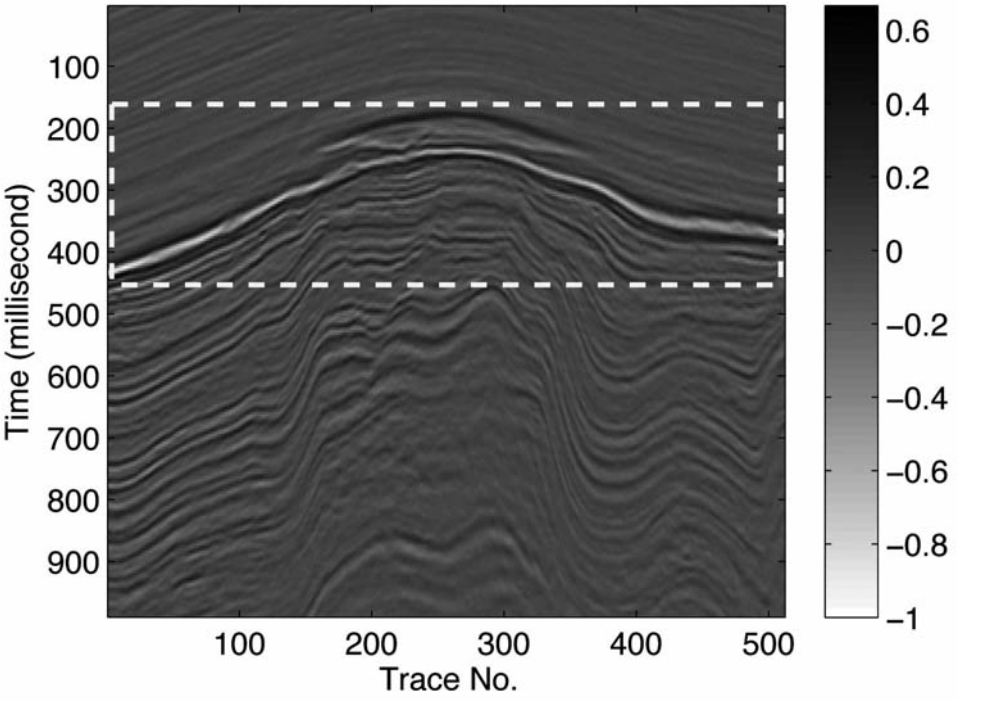

Fig. 3. A seismic section from a gas reservoir of Iran. The reservoir level is remarked by white rectangle.

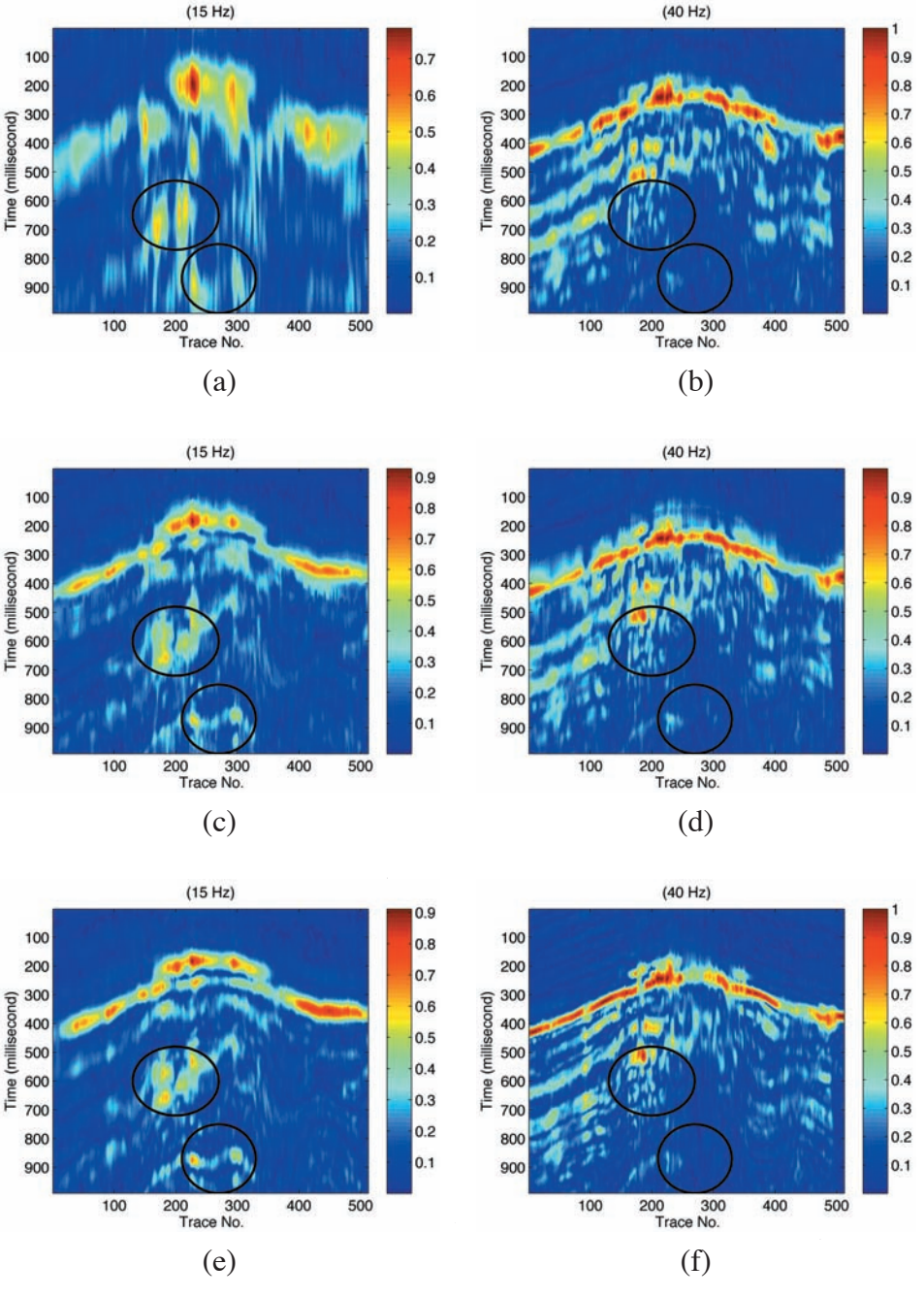

Fig. 4. Single-frequency attributes extracted from seismic section shown in Fig. 3, with 15 Hz frequency [(a), (c) and (e)] and 40 Hz frequency [(b), (d) and (f)]. The results are obtained by SST (top), the time-domain optimized TFR (middle) and the proposed method (bottom). The black ellipses remark low-frequency shadow zones.

the entire section confirm this claim. As mentioned above, regardless of geophysical effects such as imaging problems, the frequency anomalies can be caused by subsurface condition such as hydrocarbon existence. Therefore, the zones beneath the reservoir level highlighted with black ellipses in Figs. 4(a), 4(c) and 4(e) might be the low-frequency shadows. The main reason for this interpretation is that these zones have disappeared from single-frequency sections with higher frequency (Sinha et al., 2005; Castagna et al., 2003), as seen in Figs. 4(b), 4(d) and 4(f). The anomalous high amplitudes at the reservoir level can be interpreted as the gas accumulation associated with Class III type AVO anomalies (Rutherford and Williams, 1989). Other high amplitude anomalies in the single-frequency sections, both 15 Hz and 40 Hz, can be attributed to thin beds tuning effect, according to the results of the similar studies presented by Sinha et al. (2005) and Marfurt and Kirlin (2001). A well control is generally needed for more accurate interpretation.

As mentioned before a remarkable advantage of the proposed method of generating single-frequency data set is its computational speed. As an experiment, we computed run times required to extract single-frequency data set from seismic data shown in Fig. 3 using SST, the time-domain optimized TFR method and the proposed method. The computations are performed by a desktop computer with 2.26 GHz CPU and 4 Gigabytes physical memory and the algorithms are programmed in the MATLAB 7.9.0. The results are presented in Table 1. According to the results, the proposed method is performed with a significantly less run time rather than the time-domain optimized TFR method. Therefore, even if the higher resolution of the proposed method rather than time-domain optimized TFR method would not be so significant, as shown in Fig. 4, the comparison of the observed run time confirms the superiority of the proposed method. As seen in the Table 1, SST is faster than the proposed method, however, the resolution of the single-frequency seismic sections obtained by SST is significantly lower than the results of the proposed method, as seen in Fig. 4.

Table 1. The observed run-time for extracting single-frequency sections from 2D seismic data set shown in Fig. 3.

TFR method	Run time in seconds
SST	0.04
time-domain optimized TFR	228
proposed method	0.72

Channel detection

Another application of TF analysis of seismic data is channel detection (e.g., Torrado et al., 2014; Liu, 2006; Liu and Marfurt, 2005; Partyka et al., 1999; Peyton et al., 1998). A channel filled with porous rocks and encased in a nonporous matrix is one of the most important targets in exploration studies. Chuang and Lawton (1995) observed that the peak frequency slightly increases as the layer thickness decreases. It has been observed that a low peak frequency corresponds to thick channels, and a high peak frequency corresponds to thin channels (Marfurt and Kirlin, 2001). Then single-frequency data set obtained by TF analysis of seismic data set can be utilized in channel detection (Liu, 2006). In this section, for different frequencies, we obtained single-frequency seismic volumes by TFR methods of SST and the proposed method. Fig. 5(a) shows a utilized 3D seismic data set from Iran which includes 1001 in-lines and 601 cross-lines. Each seismic trace is composed of 188 time samples with 4 milliseconds sampling interval. A time-slice at 52 ms of the seismic data set is presented in Fig. 5(b) showing a main channel and two branches remarked by yellow and red arrows, respectively. The time slices at 52 ms of the single-frequency cubes for frequencies 15 Hz and 35 Hz are presented in Fig. 6. The results are obtained by SST [Figs. 6(a) and 6(b)], the time-domain optimized TFR method [Figs. 6(c) and 6(d)] and the proposed method [Figs. 6(e) and 6(f)]. The single-frequency time slices obtained by the proposed method has fewer speckle than those obtained by SST, and channels are better visualized. As seen in Figs. 6(a), 6(c) and 6(e) related to 15 Hz frequency, main channel is observed with a high amplitude while the channel branches are visible

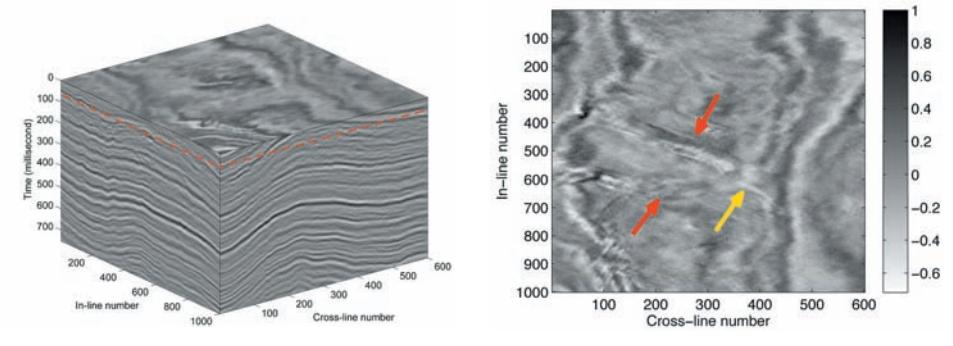

Fig. 5. A seismic data volume (a) acquired at Iran and a time slice at 52 ms remarked by red dash line on (a). A main channel and two branches are remarked with yellow and red arrows, respectively.

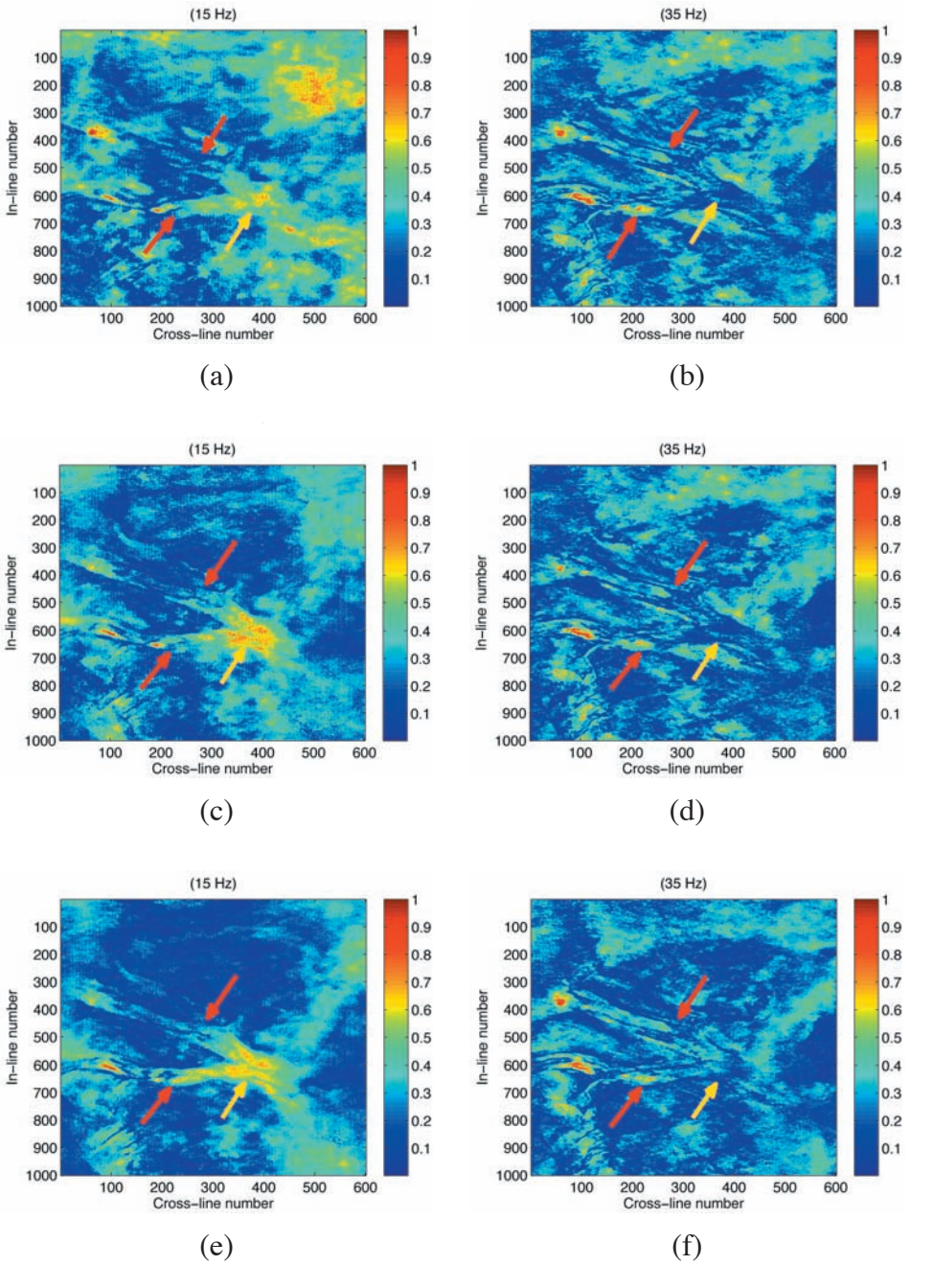

Fig. 6. Time slice at 52 ms of single-frequency cubes with 15 Hz frequency [(a),(c) and (e)] and 40 Hz frequency [(b), (d) and (f)] extracted from seismic data shown in Fig. 5. The results are obtained by SST (top), the time-domain optimized TFR (middle) and the proposed method (bottom). The yellow and red arrows remark main channel and channel branches, respectively.

with lower amplitude. In 35 Hz single-frequency time slices shown in Figs. 6(b), 6(d) and 6(f) the channel branches are well visible and the main channel has been rather disappeared. Therefore, according to Liu (2006) and Marfurt and Kirlin (2001), it seems that the main channel is thicker than channel branches because of its higher amplitude in single-frequency time slice with the lower frequency and lower amplitude in single-frequency time slice with to higher frequency.

The observed run times for generating single-frequency data set extracted from seismic volume shown in Fig. 5(a) using SST, the time-domain optimized TFR and the proposed method are presented in Table 2. As seen the run time for the time-domain optimized TFR is very high (158,520 seconds) and almost it seems not to be reasonable to employ this method for this type of application. The proposed method, with run time of 606 seconds, is significantly faster compared with the time-domain optimized TFR. The least observed run time is for SST, although, the single-frequency data set obtained by this method has lower resolution compared with the time-domain optimized TFR and the proposed method, as shown in Fig. 6.

Table 2. The observed run time for extracting single-frequency volume from 3D seismic data set shown in Fig. 5(a).

TFR method	Run time in seconds
SST	38
time-domain optimized TFR	158,520
proposed method	606

CONCLUSION

In this paper a fast technique for obtaining high resolution single-frequency seismic attributes was proposed. It was shown that, for a given signal, a high resolution TFR can be obtained by defining an optimization algorithm to find optimum window widths at each frequency component. Application of the proposed TFR method on a synthetic signal confirmed its performance in providing a high energy concentration TF map. According to the proposed TFR method to generate a high resolution single-frequency seismic data set for an interested frequency component it is sufficient to find optimum window width for that frequency component of the seismic traces. The proposed method was applied on a seismic data set to detect gas bearing zones and low-frequency shadows and also to detect channels in another data set. Results

proved the superiority of the proposed method with respect to SST in providing high resolution single-frequency data set. Afterwards, the computations showed that the proposed method is faster than the time-domain optimized TFR method for generating high resolution single-frequency attributes.

REFERENCES

Barnes, A.E., 1992. Another look at NMO stretch. Geophysics, 57: 749-751.

Castagna, J.P., Sun, S. and Seigfried, R.W., 2003. Instantaneous spectral analysis: detection of low-frequency shadows associated with hydrocarbons. The Leading Edge, 22: 120-127.

Chuang, H. and Lawton, D.C., 1995. Frequency characteristics of seismic reflections from thin beds. Can. J. Explor. Geophys., 31: 32-37.

Deng, J., Han, D., Liu, J. and Yao, Q., 2007. Application of spectral decomposition to detect deepwater gas reservoir. Expanded Abstr., 77th Ann. Internat. SEG Mtg., San Antonio.

Dilay, A. and Eastwood, J. 1995. Spectral analysis applied to seismic monitoring of thermal recovery. The Leading Edge, 14: 1117-1222.

Djurovic, I., Sejdic, E. and Jiang, J. 2008. Frequency-based window width optimization for S-transform. Int. J. Electron. Comm., 62: 245-250.

Ebrom, D., 2004. The low-frequency gas shadow on seismic sections. The Leading Edge, 23: 772.

Gholami, A., 2013. Sparse time-frequency decomposition and some applications. IEEE Transact. Geosci. Remote Sens., 51: 3598-3604.

Herrera, R.H., Han, J. and van der Baan, M., 2014. Applications of the synchrosqueezing transform in seismic time-frequency analysis. Geophysics, 79(3): V55-V64.

Hurley, N. and Rickard, S., 2009. Comparing measures of sparsity; Information Theory. IEEE Transact., 55: 4723-4741.

Jones, D. and Parks, T., 1990. A high resolution data-adaptive time-frequency representation. IEEE Transact. Acoust. Speech Signal Proc., 38: 2127-2135.

Liu, E., Chapman, M., Luizou, N. and Li, X., 2006. Applications of spectral decomposition for AVO analyses in the west of Shetland. Expanded Abstr., 76th Ann. Internat. SEG Mtg., New Orleans.

Liu, G., Fomel, S. and Chen, X., 2011. Time-frequency analysis of seismic data using local attributes. Geophysics, 76(6): P23-P34.

Liu, J., 2006. Spectral decomposition and its application in mapping stratigraphy and hydrocarbons. Ph.D. thesis, University of Houston, Houston.

Liu, J. and Marfurt, K.J., 2005. Matching pursuit decomposition using morlet wavelets. Expanded Abstr., 75th Ann. Internat. SEG Mtg., Houston: 786-789.

Marfurt, K.J. and Kirlin, R.L., 2001. Narrow-band spectral analysis and thin-bed tuning. Geophysics, 66: 1274-1283.

Odebeatu, E., 2006. Application of spectral decomposition to detection of dispersion anomalies associated with gas saturation. The Leading Edge, 25: 206-210.

Partyka, G.A., Gridley, J. and Lopez, J., 1999. Interpretational applications of spectral decomposition in reservoir characterization. The Leading Edge, 18: 353-360.

Peyton, L., Bottjer, R. and Partyka, G.A., 1998. Interpretation of incised valleys using new 3-D seismic techniques: A case history using spectral decomposition and coherency. The Leading Edge, 17: 1294-1298.

Pinnegar, R.C. and Mansinha, L., 2003. The S-transform with windows of arbitrary and varying shape. Geophysics, 68: 381-385.

Rutherford, S.R. and Williams, R.H., 1989. Amplitude-versus-offset variations in gas sands. Geophysics, 54: 680-688.

Sattari, H., Gholami, A. and Siahkoohi, H.R., 2013. Seismic data analysis by adaptive sparse time-frequency decomposition. Geophysics, 78(5): V207-V217.

Sinha, S., Routh, P.S., Anno, P.D. and Castagna, J.P., 2005. Spectral decomposition of seismic data with continuous-wavelet transform. Geophysics, 70(6): P19-P25.

Stankovic, L., 2001. A measure of some time-frequency distributions concentration. Sign. Process., 81: 212-223.

Stockwell, R.G., Mansinha, L. and Lowe, R., 1996. Localization of the complex spectrum: The S-transform. IEEE Trans. Signal Process., 44: 998-1001.

Taner, M.T., Koehler, F. and Sheriff, R.E., 1979. Complex seismic trace analysis. Geophysics, 44: 1041-1063.

Taner, M.T. and Sheriff, R.E., 1977. Application of amplitude, frequency, and other attributes to stratigraphic and hydrocarbon determination. In: Payton, C.E. (Ed.), Seismic Stratigraphy-Applications to Hydrocarbon Exploration. AAPG Memoir, 26: 301-327.

Torrado, L., Mann, P. and Bhattacharya, J., 2014. Application of seismic attributes and spectral decomposition for reservoir characterization of a complex fluvial system: Case study of the carbonera formation, Llanos Foreland Basin, Colombia. Geophysics, 79(5): B221-B230.

Wang, Y., 2007. Seismic time-frequency spectral decomposition by matching pursuit. Geophysics, 72: V13-V20.

Wang, Y., 2010. Multichannel matching pursuit for seismic trace decomposition. Geophysics, 75: V61-V66.

Wu, X. and Liu, T., 2009. Spectral decomposition of seismic data with reassigned smoothed pseudo Wigner-Ville distribution. J. Appl. Geophys., 68: 386-393.

Xue, Y.J., Cao, J.X. and Tian, R.F., 2013. A comparative study on hydrocarbon detection using three EMD-based time-frequency analysis methods. J. Appl. Geophys., 89: 926-951.

Yilmaz, O., 2001. Seismic Data Analysis. SEG, Tulsa, OK.

Zhang, Z., 2011. Spectral decomposition using S-transform for hydrocarbon detection and filtering. M.Sc. thesis, Texas A&M University, College Station.